Multiporosity in Dried Poly(vinylidene fluoride)−Camphor Systems: Effect of Drying Method on Porosity

Debarshi Dasgupta and Arun K. Nandi*

Polymer Science Unit, Indian Association for the Cultivation of Science, Jadavpur, Kolkata 700032, India

Received November 25, 2006; Revised Manuscript Received January 24, 2007

ABSTRACT: Extraction of camphor from poly(vinylidene fluoride) (PVF_2)−camphor systems prepared at two different compositions (10% and 40% w/w) indicates multiporosity. Two methods were applied for the extraction process : (i) by applying vacuum (10^{-3} mmHg) (VD) and (ii) by replacement of the host matrix by cyclohexane followed by drying (CD). The morphology, porosity, structure, and thermal properties of these samples were studied by field emission scanning electron microscopy (FESEM), atomic force microscopy (AFM), mercury intrusion porosimetry (MIP), nitrogen adsorption porosimetry (BET adsorption isotherm), wide-angle X-ray scattering (WAXS), and differential scanning calorimetry (DSC). High-pressure (20−34 000 psi) MIP histograms for all the samples indicate the presence of meso- and macropores, and low-pressure (0.5−50 psi) MIP histograms indicate the presence of large macropores in the samples. Analysis of pore size distribution from nitrogen adsorption studies by the Horvath−Kawazoe (HK) and Barett−Joyner−Halenda (BJH) models indicates the presence of micro- and mesopores produced from single, double, or multiple camphor layers between the PVF_2 strands particularly for CD samples. Pore diameter values nearly equal to the model value of 2:1 and 4:1 compounds were detected for both the single- and double-camphor layer complexation in the dried samples. However, vacuum-dried samples (P-10VD and P-40VD, the numerical numbers indicate weight percent of polymer in the gel from where it is derived) do not exhibit existence of any micropore. Mesopores were observed in all the samples although the pore size distribution is broader in VD samples than that in CD samples. The macropores are larger in size in the P-10VD samples compared to that in P-10CD samples, but in the P-40VD sample the macropore size is either reduced or lost. The hysteresis loops indicate the presence of interconnectivity between the pores, and it is lesser in the vacuum-dried samples. The surface area has greatly decreased in VD samples compared to that in CD samples. This suggests that on vacuum drying a large amount of porosity and interconnectivity is lost than those of CD samples. A schematic model is presented for the loss of porosity in vacuum drying. The crystal structure is independent of drying method, and the melting point of the porous surface increases in VD samples compared to that in CD samples, indicating that thicker porous surface is produced on vacuum drying. The collapsing of pores decreases the porosity in VD samples due to mechanical jerking. Honeycomb-type pores are observed in the P-40CD sample, and the faster crystallization rate of camphor than that of PVF_2 has been attributed to the honeycomb-type pore formation. The sheetlike morphology of PVF_2 obtained from dried dilute gels has been attributed to its crystallization through the niches of camphor crystals followed by extraction of camphor.

Introduction

Recently, porous materials have drawn a significant research interest because of its increased use in catalysis, superadsorbents, ion exchange resins, size selective separation, ultralow dielectric materials, templates for synthesis of nano-objects, antibody or enzyme immobilization, sorption processes, etc.[1−10] For different uses porous materials of different pore diameters and different chemical characteristics are required. According to IUPAC classification, pores may be classified as micro, meso, and macro for their diameters <2, 2−50, and >50 nm, respectively.[2,11] The presence of all the pores in the same material is called multiporous materials.[12−16] The multiporous materials have many applications such as chromatography, drug release, and separation of large molecules.[2,15,16] Such structures provide a high surface area and at the same time minimize the pressure drop over the material.[16] Microfluidic-based sensors use multiporous material where large sized pores (hundreds of nanometers) are useful for microfluidic flow control and the small sized pores (tens of nanometers) are useful for increasing device surface area to achieve fast response time and high sensitivity.[15] The multiporous materials find great application in systems where optimization of diffusion and confinement regimes is required.[2] Micro- and mesopores provide the size and shape selectivity for the guest molecules, and the macroporous channels permit improved access to the active sites avoiding pore blocking by reagents or products. Though there are examples of some inorganic multiporous materials,[15−20] the polymeric multiporous materials are yet very few.[12−14]

Recently, Guenet et al.[21] proposed that multiporosity of nanometer and subnanometer dimensions might be achieved by drying of thermoreversible gels, and we reported the preparation of multiporous polymeric materials from careful drying of thermoreversible poly(vinylidene fluoride) (PVF_2)−diester gels keeping the gel structure intact.[12,13] PVF_2−diester gels were dried by replacing the gelling medium with a low boiling guest solvent which should be close to the Θ solvent. However, such a solvent replacement process is lengthy and tedious, and a solid but volatile solvent camphor, producing thermoreversible gel with PVF_2, reported earlier,[22] may be easier to extract by vacuum drying. Camphor is a bicyclic compound (1,7,7-trimethylbicyclo[2,2,1]heptane-2-one) that contains a $\rangle C{=}O$ group having an interaction with $\rangle CF_2$ dipole of PVF_2.[23,24] It was demonstrated in our earlier work that the above interaction exists in the PVF_2−camphor system producing incongruently melting polymer−solvent complexes of two different stoichiometries (monomer unit of PVF_2:camphor = 2:1 and 4:1).[22]

* Corresponding author. E-mail: psuakn@mahendra.iacs.res.in.

10.1021/ma062709h CCC: $37.00
Published on Web 02/22/2007

Scheme 1. (a) An Approximate Molecular Model of Single-Layer Camphor Complexation between Two PVF_2 Strands in PVF_2 Camphor Complex (PVF_2 Monomer:Camphor = 2:1) Obtained by Energy Minimization Using MMX Program; (b) An Approximate Molecular Model of Bilayer Camphor Complexation between PVF_2 Strands in PVF_2−Camphor Complex (PVF_2 Monomer:Camphor = 2:1) Obtained by Energy Minimization Using the MMX Program

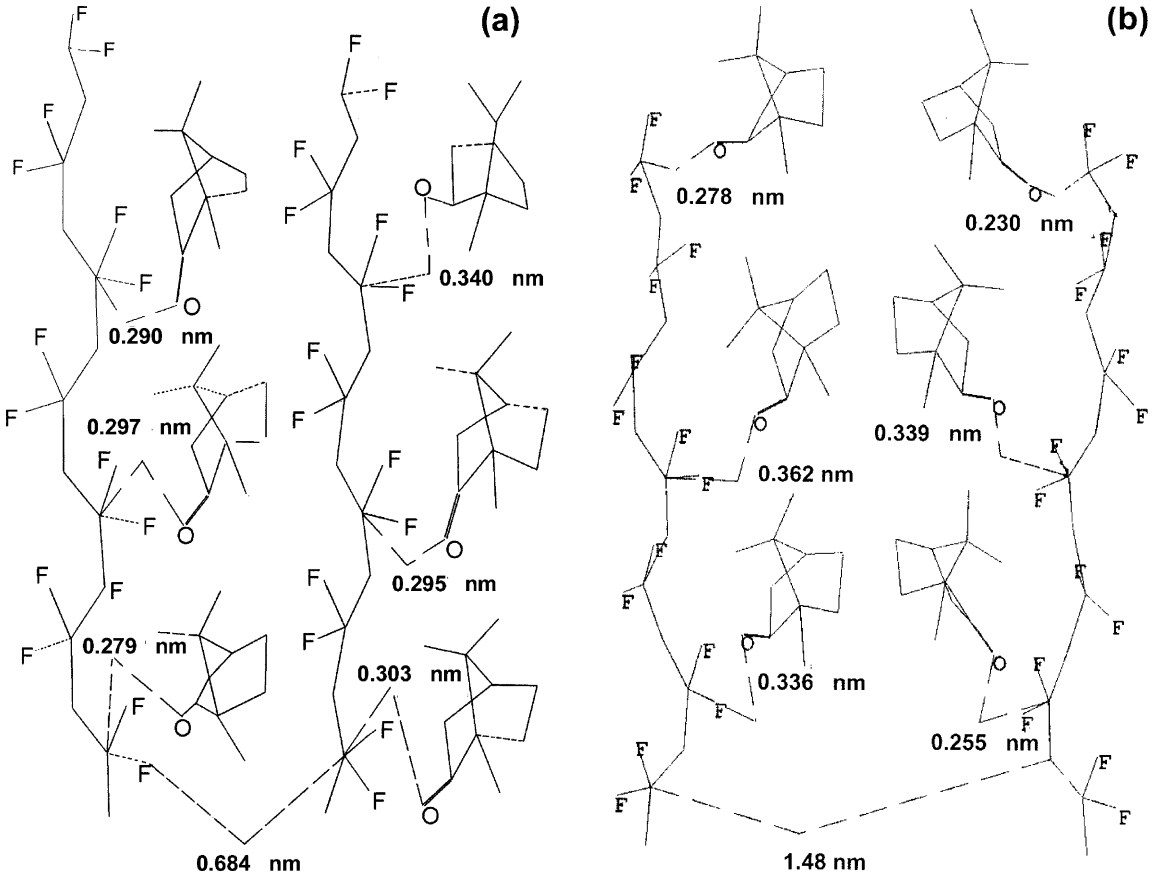

Two approximate models of the 2:1 complex obtained from the MMX program is presented in Scheme 1a,b for monolayer and bilayer camphor complexation between the two PVF_2 strands (see also supplementary Scheme 1a,b for the 4:1 compound in the Supporting Information). From the models it is apparent that successful removal of camphor molecules may yield micropores of diameter 0.7 and 1.5 nm, respectively, and the removal of solvent molecules is thermodynamically feasible because the incongruently melting compounds break before they melt.[25] Multiple camphor layers and interdigitation of camphor molecules in such layers would definitely yield micro- and mesopores of larger pore dimension. Further, PVF_2−camphor gels have three-dimensional network structures where camphor molecules are entrapped into the network cages producing the gel.[22] Careful removal of these entrapped camphor molecules may yield macropores.[12,13] Thus, multiporous material can be achieved after drying of the PVF_2−camphor gel.

Poly(vinylidene fluoride) is a technologically important polymer,[26] and it is much used as membrane (Millipore) forming material.[27] The commercial PVF_2 membranes have average pore diameter 570, 1410, and 1960 nm.[5] PVF_2 is hydrophobic in nature, and on grafting with poly(acrylic acid), poly(ethylene glycol), poly(methylacrylic acid), and poly(oxyethylene methacrylate) antifouling and pH-sensitive properties are introduced.[4,28] Here we would use thermoreversible PVF_2 gels to prepare multiporous materials through two different drying techniques. Drying techniques may have a certain influence on the pore size and pore size distribution because in the gel state the PVF_2 chains are not rigid enough as they are in the semisolid state. Consequently, any jerking, i.e., sudden external stress applied during drying, may destroy the pore structure present in the gel state. On applying vacuum there is a probability of jerking, which may collapse pores. To test this proposition the PVF_2−camphor gels were dried both by vacuum and by the solvent replacement method using cyclohexane as in PVF_2 diester gels.[12,13] Cyclohexane is chosen as guest solvent because its approximate diameter is 5 Å so it would not destroy the layer structure (Scheme 1), and it is also very close to Θ solvent of PVF_2, rendering its conformation unaffected during the extraction.[13] In this paper we have compared the pore size distribution obtained by these two methods together with the morphology of the pores obtained from field-emission scanning electron microscopy. Thus, the present study is important to rationalize the minimum and maximum size pores present in the dried gels and the influence of the drying method on the porosity of the gels. Both camphor and PVF_2 are crystalline, and during cooling from their melt there is a chance of competitive crystallization, which may influence the gel structure and hence pore morphology. Here an attempt is also made to understand the pore morphology from these viewpoints. We have chosen two gel compositions where the 2:1 PVF_2−camphor complex and solid solution of PVF_2 and camphor exist.[22]

Experimental Section

Samples. Poly(vinylidene fluoride) (PVF_2) is a product of Aldrich Chemical Co. Inc. The weight-average molecular weight ($\bar{M}_w$) of the sample is 1.8×10^5, and the polydispersity index is 2.54 as obtained from GPC. The sample was recrystallized from its 0.2% (w/v) solution in acetophenpne. The high molecular weight of PVF_2 would facilitate gel formation at low polymer concentration. DL-Camphor (S.D. Fine Chem Ltd., Mumbai) was purified by a sublimation procedure.

Gel Preparation. The PVF_2 and camphor with appropriate PVF_2 weight fractions (0.1 and 0.4) were taken in thick-walled glass tubes (8 mm in diameter and 1 mm thick) and were sealed. The samples in the sealed tube were melted at 210 °C in an oven for 20 min with intermittent shaking to make homogeneous. The shaking was performed in a rotor (Remi, Cyclo-Mixer). The transparent solution was then quenched to 30 °C to form the gel.

Preparation of Porous Materials. To prepare the porous materials from the gel precursors, two methods of drying were used.

(i) Vacuum Drying (VD). One portion of the gel was exposed to vacuum (10^{-3} mmHg) at 40 °C for 10−12 days. Complete removal of camphor was confirmed from the absence of the ⟩C═O peak (1741 cm^{-1}) of camphor in the FT-IR spectra of the dried samples (Figure 1 of Supporting Information).

(ii) Cyclohexane Drying (CD). The remaining portion of the gel was kept immersed in cyclohexane for 8−10 days to replace camphor by cyclohexane.[13] To drive the above replacement process quickly, the cyclohexane was replaced by a fresh batch after every 12 h. After extraction of camphor in cyclohexane, they were first dried in air and finally in vacuum at 35 °C for 3 days.

Characterization of Porous Materials. The morphology of porous samples was recorded in a field emission scanning electron microscope (FE-SEM) (JEOL, JSM-6700F). The samples were platinum coated with a layer of thickness 40 nm by a sputtering technique in an argon atmosphere and were then observed. The AFM study of the PVF_2−camphor blend and the porous material were done using a di cp-II (Veeco) instrument on topography mode. The data were processed in proscan-1.8 software. The FT-IR study was done using a Nicolet FT-IR instrument (Magna IR 750 spectrometer, Series II). The WAXS studies of the dried gels were performed by a Seifert X-ray diffractometer (C-3000) using nickel filtered Cu−Kα radiation with a parallel beam optics attachment. The instrument was operated at a 35 kV voltage, and a 30 mA current and was calibrated with standard silicon sample. The samples were scanned from $2\theta = 2°$ at the step scan mode (step size 0.03°, preset time 2 s), and the diffraction pattern was recorded using a scintillation counter detector.

The melting point and enthalpy of fusion of the dried gels were measured using a differential scanning calorimeter [Diamond DSC (Perkin-Elmer)] under N_2 atmosphere. The porous samples, encapsuled in aluminum pans, were heated from 50 to 230 °C at the rate 40 °C/min. The higher heating rate was chosen to avoid any melt recrystallization of the PVF_2 sample.[29,30] To get the cooling thermograms of PVF_2 camphor gel, the gel was taken into large volume capsule (LVC) pan and the pan was properly sealed. The LVC were used to ensure that no solvent evaporation takes place during the melting of the gel. The gel was then melted to 210 °C and cooled at a rate of 5 °C/min. The thermograms were analyzed with a personal computer using Pyris software (version 7.0). The instrument was calibrated with cyclohexane and indium standard in the whole temperature range before experiment. The uncertainity in the melting point and crystallization temperature measurements is ±0.05 °C.

Porosity Measurement. For porosity measurement both mercury intrusion porosimetry (MIP) and N_2 adsorption porosimetry were used. The former was used to measure pore diameter > 6 nm, and for pore diameter < 6 nm the N_2 adsorption method was used.

Mercury intrusion porosimetry is based on the principle that nonwetting liquids intrude into the capillaries under pressure (P) following the Washburn equation[31]

$$r = \frac{-2\gamma \cos\theta}{P} \tag{1}$$

where r is the radius of the pore, γ is the surface tension, and θ is the contact angle of mercury (nonwetting liquid) with the solid sample. The fraction of volume per unit mass occupied by the pores having radii in the interval (r and $r + dr$) can be deduced from the volume of mercury that intrudes within the pressure range (P and $P + dP$)

$$dV = -D_V(r)\, dr \tag{2}$$

where $D_V(r)$ refers to the volume pore size distribution function defined as the pore volume per unit interval of pore radius per unit of mass. Combiniing eq 1 and eq 2,[32] we have

$$D_V(r) = \left(\frac{P}{r}\right)\frac{dV}{dP} \tag{3}$$

Here we have plotted both the normalized pore volume and $D_V(r)$ with pore diameter.

The mercury intrusion porosimetry was done using the instrument Poremaster 33 (Quantachrome Instrument). Two pressure ranges were applied; e.g., low-pressure range (0.5−50 psi) was used to measure pores >10 μm and high-pressure range (20−34 000 psi) was used to measure pore size <10 μm. Blank correction was made using α-Al_2O_3 beads. The sample was introduced in a penetrometer having stem volume 0.5 cm^3 and was at first kept at the low-pressure chamber, and both intrusion and extrusion runs were recorded. After completion of the experiment the penetrometer was taken out from the low-pressure chamber and transferred to a high-pressure chamber with the replacement of a little mercury at the stem by silicon oil, and the pressure was applied by hydraulic means. The data were analyzed by Porowin-32 software. The nitrogen adsorption porosimetry was done with Quantachrome Autosorb 1-2C instrument (Quantachrome Instruments). The surface area of the porous samples was determined from the BET function. To measure the pore size and pore size distribution of the mesopores and micropores, the BJH (Barett−Joyner−Halenda)[33] and HK (Horvath−Kawazoe)[34] methods were used respectively using Autosorb 1 software.

Results and Discussion

Porosity. 1. 10% PVF_2−Camphor Gel. In Figure 1a,b the FESEM micrographs of cyclohexane-dried (CD) and vacuum-dried (VD) PVF_2−camphor gels are compared. In the micrographs, sheetlike morphology with pores of different dimensions is observed in both the cases. Qualitatively, the sheets of CD samples are of smaller size than that of VD samples, suggesting that in VD samples the sheets appear to be joined together. The micrograph and the inset of Figure 1a indicate that there are medium and smaller size pores, whereas in Figure 1b the pore sizes are larger. In other words, smaller pores present in CD samples are collapsed to produce the larger size sheets and larger size pores in the VD sample. To get a quantitative picture of porosity, the MIP histograms of both the samples are compared in Figure 2a,b both for high-pressure and low-pressure runs. Comparison of the histograms is made in the same scale though the scales for high-pressure and low-pressure histograms are different. There are pores with dimension 6 nm to 400 μm in all the samples, indicating that multiscale porosity is present in both cyclohexane and vacuum-dried 10% (w/w) PVF_2 camphor gels. It is noteworthy that both the high-pressure and low-pressure histograms are not of similar type for P-10VD and P-10CD samples. From the low-pressure histograms it is evident that in the P-10VD sample there are larger size macropores than those in P-10CD sample, and the populations of the macropores at larger diameters are greater in the P-10VD sample than those in P-10CD samples. In high-pressure histograms the CD sample has a sharper size distribution of the pores while in VD sample the distribution is broader. To compare the pore size of VD and CD samples more quantitatively, the pore size distribution curves are presented in Figure 3. It is apparent from the figure that the maximum value of distribution function is larger in the CD sample than that in the VD sample which shows a doublet peak. These indicate that pore volume per unit pore diameter interval is larger in the CD samples compared to those of the

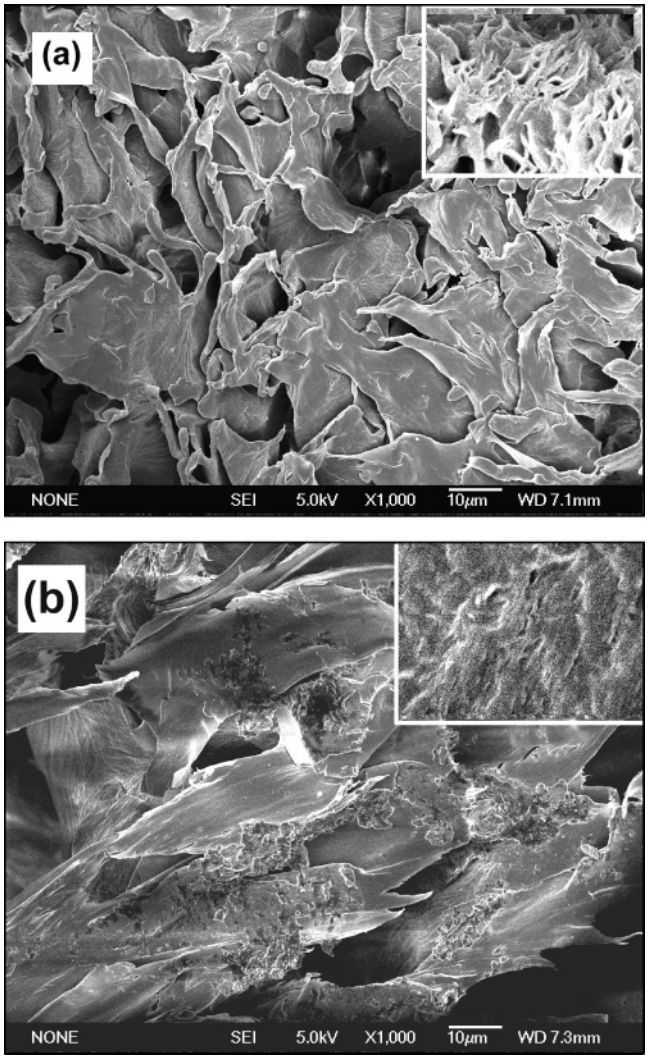

Figure 1. FESEM micrographs of **(**a**)** P-10CD [inset of (a**)**: 10 times magnified picture] and **(**b**)** P-10VD [inset of (b): 10 times magnified picture] samples.

VD samples. The CD sample may have another peak at lower pore diameter value as apparent from the distribution curve, and its height is higher than that at 8 nm. Because of the limitation of the instrument, this is only partly observed. It is also noteworthy that the distribution of peaks are shifted to higher pore diameter in the VD sample compared to those of the CD sample; these results signify some smaller sized pores present in the gel structure are transformed into new larger diameter pores on vacuum drying. In the inset of Figure 3 the low-pressure distribution curves of P-10VD and P-10CD samples are compared, and it certainly signifies that in the VD sample the distribution function of macropores is drastically reduced together with a shift of the peak to higher pore diameter. So it may be concluded from these results that porosities from 6 nm to 400 μm are present in the samples, and some change in pore structure is occurring during vacuum drying than those in the cyclohexane drying method.

MIP has the limitation that it cannot measure the pore diameter less than 6 nm. To understand the presence of micro- and mesopores and the effect of drying method more vividly in these region, the nitrogen adsorption porosimetry experiments were performed, and the BJH pore size distribution curves[33] are compared in Figure 4a,b for P-10CD and P-10VD samples. It is apparent from the figure that the height of the distribution peaks has significantly decreased for VD sample as compared to that of the CD sample, and the peak positions also shifted to higher diameter values. This is very similar to MIP distribution curves; i.e., the smaller size pores experience collapsing, and in lieu higher size pores are produced. The BJH method of pore size distribution has a limitation for the minimum size pore diameter of 2 nm. However, the samples may have pores of much lower diameter as predicted in Scheme 1a,b. So we have plotted HK pore size distribution curves[34] relevant for micropores, and it is evident from the figure (Figure 5) that the P-10 CD sample has pores at 0.63, 0.95, 1.42, and 1.83 nm while the P-10VD sample has no distribution in the above-mentioned pore sizes. This certainly indicates that vacuum drying destroys the micropores significantly. It should be mentioned here that the minimum pore size determined by this method is 0.63 nm, which is very close to that predicted for the single camphor layer for the PVF_2−camphor complexes (Scheme 1a and supplemental Scheme 1). The 1.42 nm peak may arise from double camphor layer (model value = 1.48 nm in Scheme 1b). The 0.95 nm peak is in between the values of single and double layer of camphor molecules and may arise from the intermediate, i.e., interdigited camphor structure. The 1.83 nm peak might be attributed for the higher ordered structure. Apart from these micropores, a large number of mesopores are generated for the intercalation of camphor molecules at the intermediate positions of camphor layered structures (Scheme 1,b). It may be argued from this study that to get micropores vacuum drying is not a suitable process, and the solvent replacement technique is good for this purpose.

2. 40% PVF_2−Camphor Gel. To observe the effect of drying method on porosity for concentrated gels ($W_{PVF_2} = 0.4$) and also to compare it with the data of dilute gels ($W_{PVF_2} = 0.1$), we have investigated the CD and VD samples of 40% (w/w) PVF_2−camphor gel. In Figure 6, the SEM micrographs of P-40VD and P-40CD samples are compared. It certainly indicates that pores in the VD sample are smaller than those in the CD sample. The pores in P-40CD sample are honeycomb-type pores. On magnification of the walls, mesopores are also observed (inset of Figure 6a). But in the P-40VD sample such pores are absent; in lieu smaller size macropores are observed. In Figure 7a a representative AFM picture of the gel indicates a continuous structure which transformed into a porous structure on proper drying (CD, Figure 7b). Pores of size 30−300 nm are clearly observed in this figure. In Figure 8 the MIP histograms of P-40CD and P-40VD samples are presented both for high-pressure and low-pressure experiments to get quantitative results. It is apparent from the figure that in the P-40CD sample pore diameter lies in the range 6 nm to 200 μm and in the P-40VD sample pore diameter only in the range of 100 nm to 2 μm exist. (Some macropores are present in the range 10−200 μm for the P-40VD sample, but its average population is only 2% of those of the P-40CD samples.) In Figure 9, the MIP pore size distribution curves of P-40CD and P-40VD samples are presented, and there exists a large difference between the two distribution curves. The CD sample has a significant number of pores of diameter in the range 10−20 nm and small number of pores in the range 300−500 nm. But in the VD samples the pores in the range 10−20 nm diameter are totally absent while pores of diameter in the range 300−500 nm exist.

To compare the smaller sized pores (<10 nm) in P-40CD and P-40VD samples, N_2 adsorption porosimetry has been done, and from the BJH distribution curves (Figure 10) it is apparent that the CD sample has very sharper distribution with pore diameters at the peak position 1.9, 2.7, 4.9, and 12.2 nm. On the contrary, the VD samples exhibit a broad peak at 3.8 nm

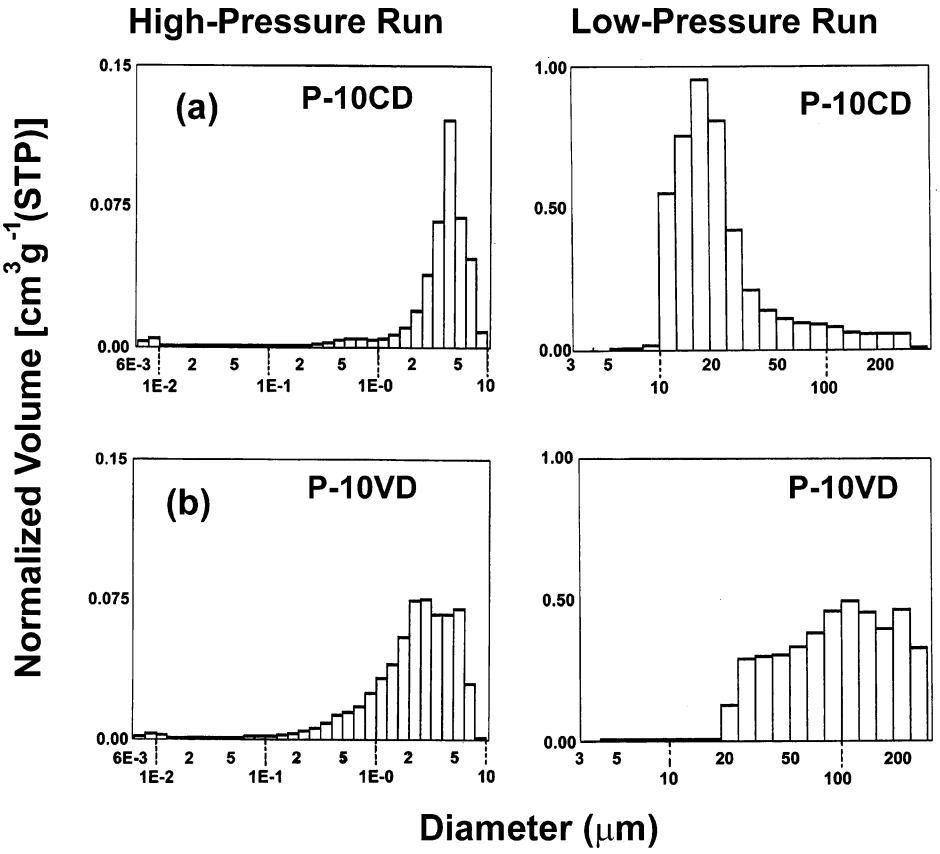

Figure 2. MIP high-pressure and low-pressure intrusion histograms of **(**a**)** P-10CD and **(**b**)** P-10VD samples.

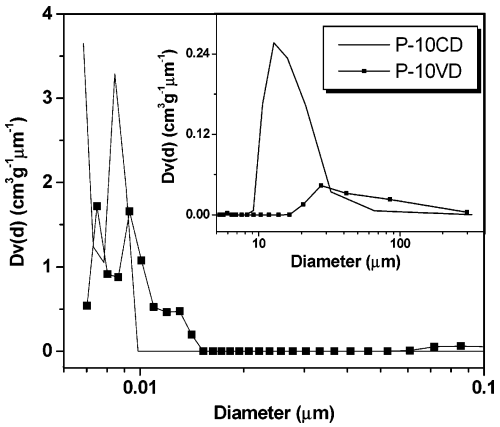

Figure 3. MIP high-pressure pore size distribution curves of P-10CD and P-10VD samples [inset: MIP low-pressure pore size distribution curves].

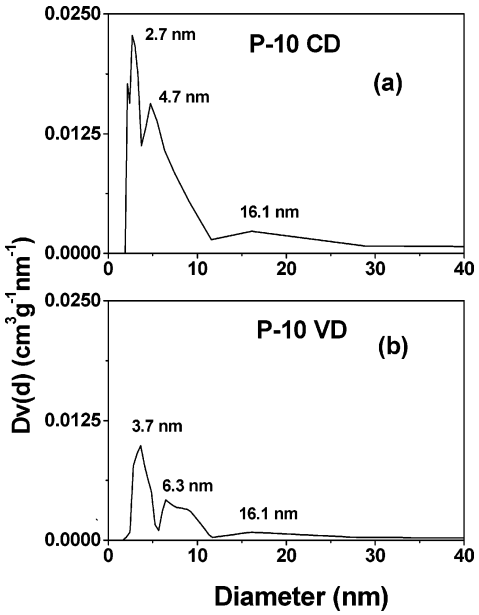

Figure 4. BJH pore size distribution curves of **(**a**)** P-10CD and **(**b**)** P-10VD samples.

with a relatively smaller peak height. These results conclude that well-organized mesopores are destroyed during vacuum drying, and new pores with wider size distribution are produced.

To compare the micropores in P-40VD and P-40CD samples, HK plots[34] are presented in Figure 11, and the figure indicates that the CD sample has pores at 0.72 and 0.84 nm. It approximately corresponds to the values of single-layer 2:1 and 4:1 PVF_2 camphor compounds (see models, Scheme 1, and supplementary Scheme 1). However, some pores of diameter 0.97, 1.09, and 1.27 nm with lesser population are also observed. The 1.27 nm peak may be related to the double camphor layer of 4:1 PVF_2 camphor compound (supplementary Scheme 1b) while no definite reason for the occurrence of 0.97 and 1.09 nm peaks is known. It might arise due to sporadic inclusion of camphor molecule on PVF_2−camphor complexes, and its concentration is much lower compared to the 0.72 and 0.84 nm diameter pores. Nonetheless, it may be concluded from the results that micropores are created by the extraction of solvent molecules from the polymer−solvent complexes; mesopores and macropores are created from the extraction of solvent molecules entrapped within the polymer network, yielding multiporosity in the sample. Here also vacuum drying destroys the micropores in this concentrated gel.

It is now pertinent to discuss here that the composition, $W_{PVF_2} = 0.4$, is almost equal to stoichiometric composition of the 2:1 complex (C_1, $W_{PVF_2} = 0.44$).[22] In this system one would expect

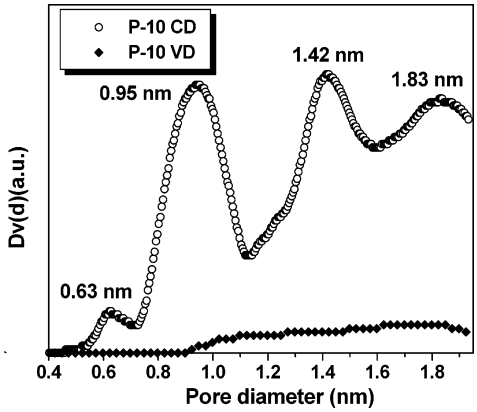

Figure 5. HK pore size distribution plots of P-10CD and P-10VD samples.

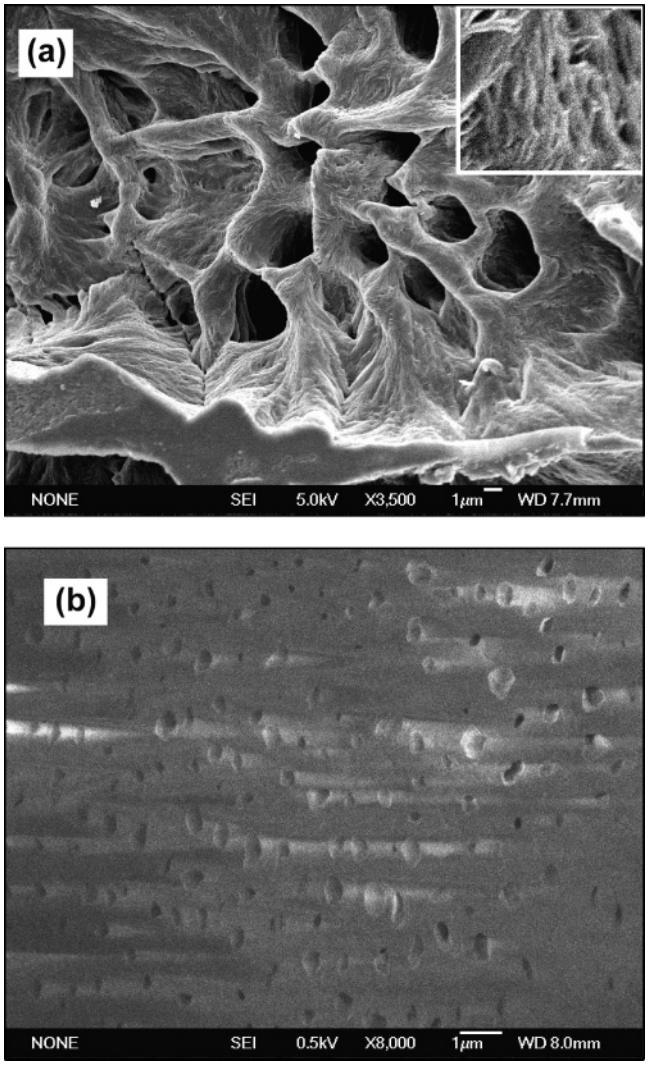

Figure 6. FESEM micrographs of **(**a**)** P-40CD sample [inset of (a): 10 times magnified picture of the pore walls] and **(**b) P-40VD sample.

only pores of model size diameter 0.68/1.48 nm, but we have observed multiporosity in this material. From WAXS result of Figure 7 in ref 22 it may be probable that thin PVF_2 α-crystallites (characteristic peaks 13.58 and 14.42 nm^{-1}) coexist with the complex (characteristic peaks 10.4, 11.0, 11.8, and 12.8 nm^{-1}). Also from the phase diagram (Figure 2 of ref 22) at this composition PVF_2−camphor solid solution exists. This would therefore yield clusters of camphor molecules of

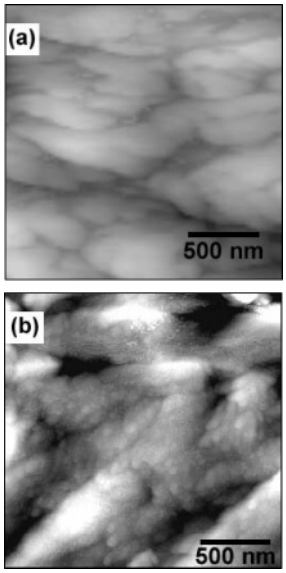

Figure 7. Representative AFM height images of (a) PVF_2−camphor gel ($W_{PVF_2} = 0.40$) and (b) P-40CD sample.

different sizes to be entrapped by PVF_2 chains apart from the complexes (solvated crystallites). Further during extraction, as composition of the complex changes it may produce the 4:1 complex, which may yield lower size micropores. The two main peaks at 0.72 and 0.84 nm in Figure 11 may arise for these reasons. Thus, multiporosity in this composition is achieved. The same explanation is also applicable to the gel composition $W_{PVF_2} = 0.1$.

Hysteresis. In Figure 12a−d the hysteresis loops of P-40CD and P-40VD samples are compared for both MIP high-pressure and low-pressure runs. The high-pressure MIP hysteresis curves clearly indicate that P-40CD sample has quite a large amount of hysteresis between the mercury intrusion and extrusion curves. This is because mercury entrapped into the pores during intrusion required much lower pressure to extrude. Such a situation occurs when there is interconnected channels between the pores or due to the presence of pores of ink-bottle-type structure.[13,35−38] In a word hysteresis indicates interconnectivity between the pores, and it may be supported from the three-dimensional percolation model obeyed by thermoreversible PVF_2 gels.[38−40] In the P-40VD sample the hysteresis is lower, indicating connectivity among the pores is much reduced. For low-pressure MIP histograms (Figure 12c,d) the difference between the hysteresis loops of the P-40 CD and P-40VD samples is very prominent. The P-40CD sample has very large amount of connectivity in larger size macropores also, but it is totally lost in the P-40VD sample. Thus, it may be concluded that in the P-40VD sample pore connectivity in both macro- and mesopores is reduced due to pore collapsing during vacuum drying.

The MIP hysteresis curves of P-10CD and P-10VD samples are presented in the supplementary Figure 2a−d. There is no appreciable connectivity at the high-pressure region for both the P-10CD and P-10VD samples, but at the low-pressure region some interconnected channel structures are evident in the P-10CD sample. In the P-10VD sample the nature of the hysteresis at low-pressure region indicates a permanent retention of mercury probably due to locking of interconnected channels. The BET adsorption isotherms of P-10CD and P-10VD samples (Figure 13a,b) indicate a large amount of connectivity in the micro- and mesopores in the P-10CD sample than that in P-10VD sample. In the BET isotherms of P-40CD and P-40VD

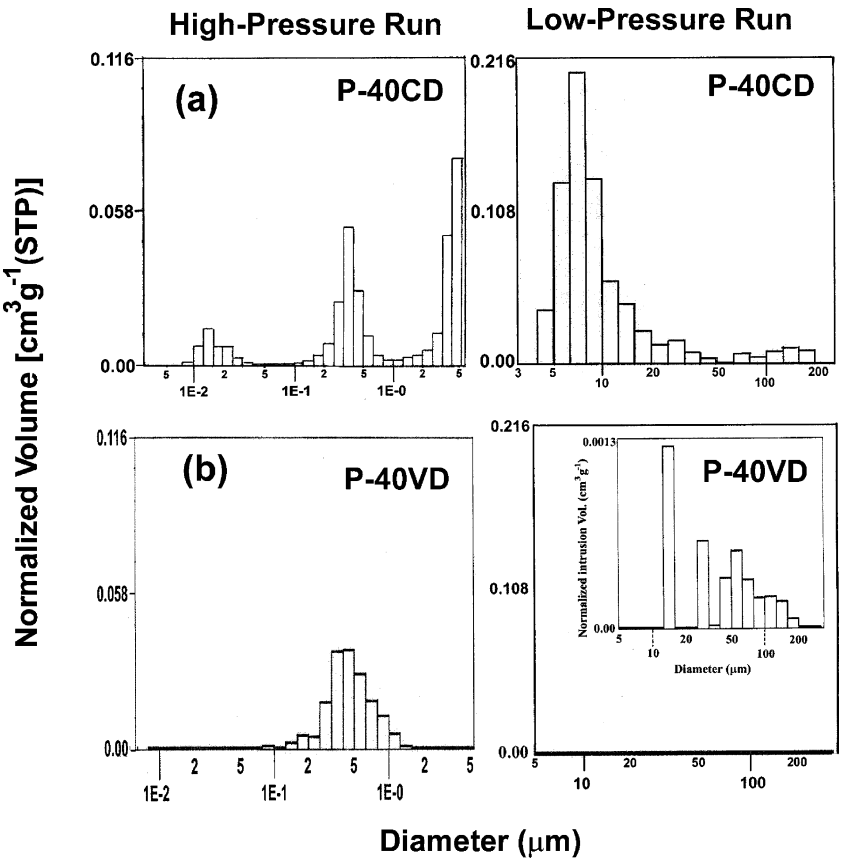

Figure 8. MIP high-pressure and low-pressure intrusion histograms of **(**a**)** P-40CD and **(**b**)** P-40VD samples [inset of (b): enlarged *Y*-axis of low-pressure histogram showing much less population (2% of CD samples) of macropore].

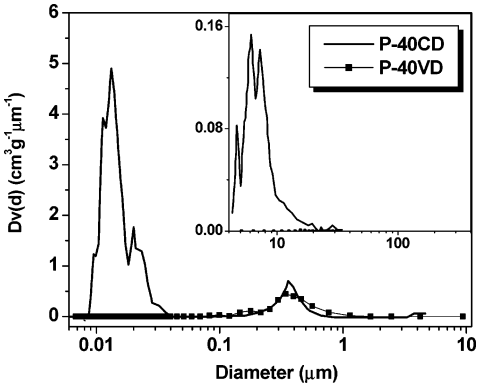

Figure 9. MIP high-pressure pore size distribution curves of P-40CD and P-40VD samples. Inset: low-pressure distribution curves.

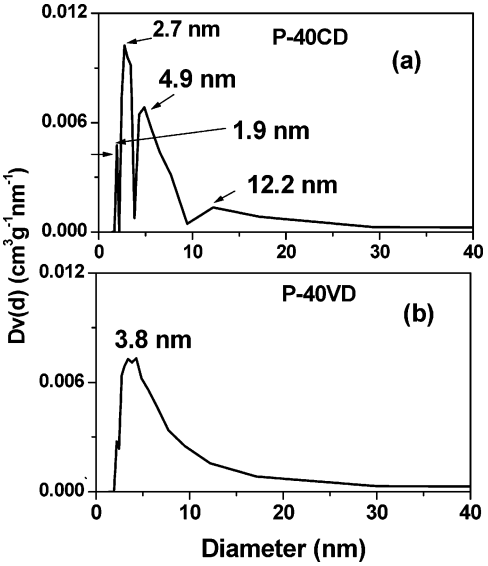

Figure 10. BJH pore size distribution curves of **(**a**)** P-40CD and **(**b**)** P-40VD samples.

samples the hysteresis is very low for the former, and it is totally absent in the latter sample (supplementary Figure 3). So it may be concluded from these results that the method of drying has significant influence not only on the porosity (pore diameter and pore concentration) of the samples but also on the connectivity between the pores. The vacuum drying significantly decreases both porosity and connectivity of the pores than those of cyclohexane-dried samples.

Structure and Thermal Property. The influence of drying method on the structure of porous materials is discussed here. The WAXS patterns of the CD and VD samples (supplementary Figure 4) indicate that α-crystalline polymorph is produced in both samples.[41−43] So there is no influence of drying method and gel composition on the structure of the porous materials. It is pertinent to discuss here that the WAXS pattern of the PVF_2−camphor system obtained from synchrotron radiation exhibits new peaks for the PVF_2−camphor complexation at $q = 10.4$, 11, 11.8, and 12.8 nm^{-1} together with the presence of α-crystalline peaks of PVF_2 at $q = 13.58$ and 14.42 nm^{-1} (Figure 7 in ref 22). One scenario that is consistent with the data, but not yet proven, is the coexistence of the layers of α-crystallites of PVF_2 and its complexes side by side; probably, the complexation occurs on the thin crystallite surfaces mentioning the stoichiometric composition. The presence of solid solutions of PVF_2 and camphor may be another cause for the above WAXS pattern. On drying by vacuum or by solvent replacement technique the camphor molecules of polymer−solvent complexes as well as camphor molecules entrapped by the solvated crystallites are

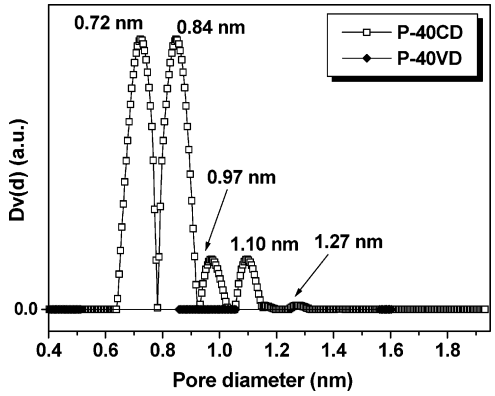

Figure 11. HK pore size distribution plots of P-40CD and P-40VD samples.

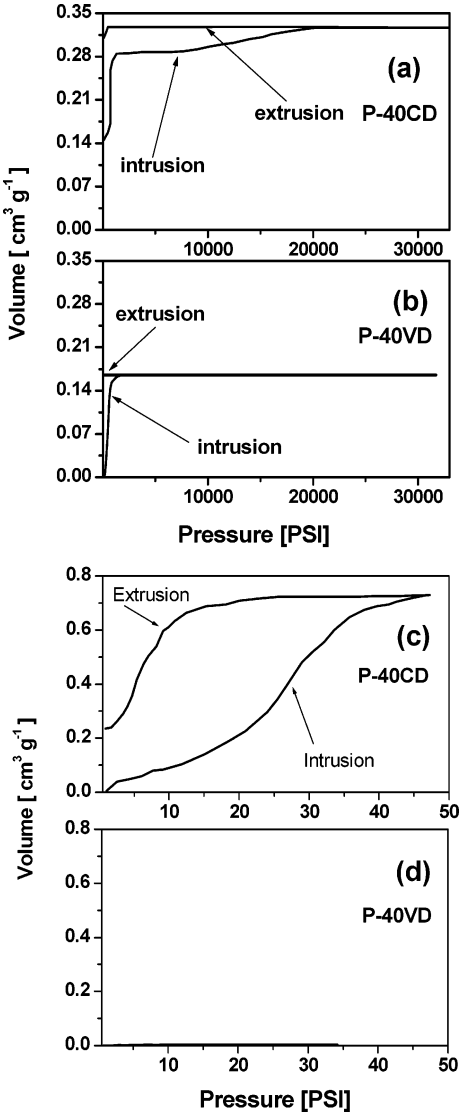

Figure 12. (a ,b) MIP high-pressure hysteresis between mercury intrusion (lower curve) and extrusion (upper curve) for **(**a**)** P-40CD and **(**b**)** P-40VD samples. **(**c, d) MIP low-pressure hysteresis between mercury intrusion (lower curve) and extrusion (upper curve) for **(**a**)** P-40CD and **(**b**)** P-40VD samples.

extracted, and only the α-crystalline peaks of PVF_2 are obtained. Because of the extraction, some change in intensity ratios of the peaks than the respective peaks of melt cooled α-polymorph PVF_2 is observed, and this may arise from the polymer−solvent complexation.[22]

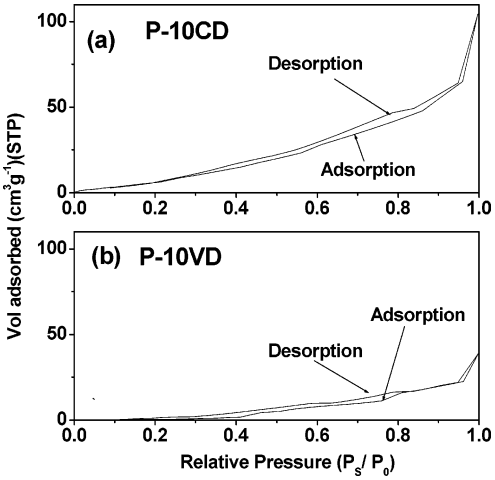

Figure 13. BET adsorption (lower curve) and desorption (upper curve) isotherms for **(**a**)** P-10CD and **(**b**)** P-10VD sample.

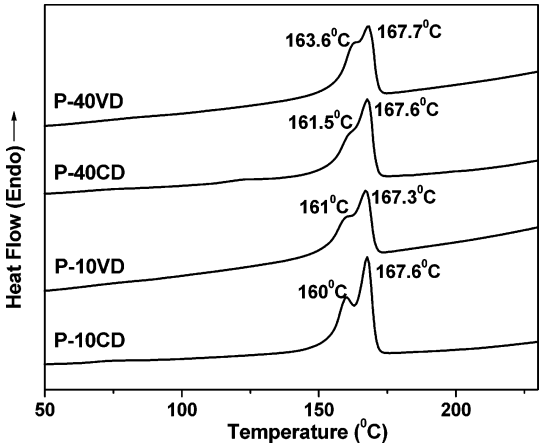

Figure 14. DSC heating thermograms of CD and VD samples at the indicated compositions at the heating rate 40 °C/min.

Table 1. Pore Volume and Surface Area of CD and VD Samples of PVF_2−Camphor Gels in Two Concentrations of Polymer, Namely 10% (w/w) and 40% (w/w)

	pore volume (cm^3 /g)				surface area (m^2/g)		
	BJH	MIP					
sample	<6 nm	high pressure	low pressure	total	BET	MIP	total
P-10CD	0.07	0.41	4.40	4.88	58.04	3.68	61.72
P-10VD	0.02	0.61	4.31	4.94	4.13	4.25	8.38
P-40CD	0.03	0.33	0.71	1.07	32.65	11.80	44.45
P-40VD	0.028	0.16	0.004	0.19	12.32	1.62	13.94

It is apparent from the thermograms (Figure 14) that there are two peaks even at the higher heating rate (40°C/min), indicating the probability for the presence of two types of PVF_2 crystal in the porous materials. This lower melting peak may arise due to the crystals at porous surface, and due to the large surface area of these crystals the melting point is lower.[13,44] On the other hand, the higher melting peak may arise due to the melting of bulk PVF_2 crystal, and its higher melting point is due to the thicker crystals at bulk. These peaks are not arising due to melt recrystallization for the formation of thicker lamella crystals from thinner lamella crystals (metatectic phase behavior) as the thermograms texture do not change with heating rate (supplementary Figure 5). It is apparent from the thermograms that the melting points of lower melting peaks increase with increasing concentration, indicating higher concentrated gels produces thicker pore surface. Also, the lower melting peaks

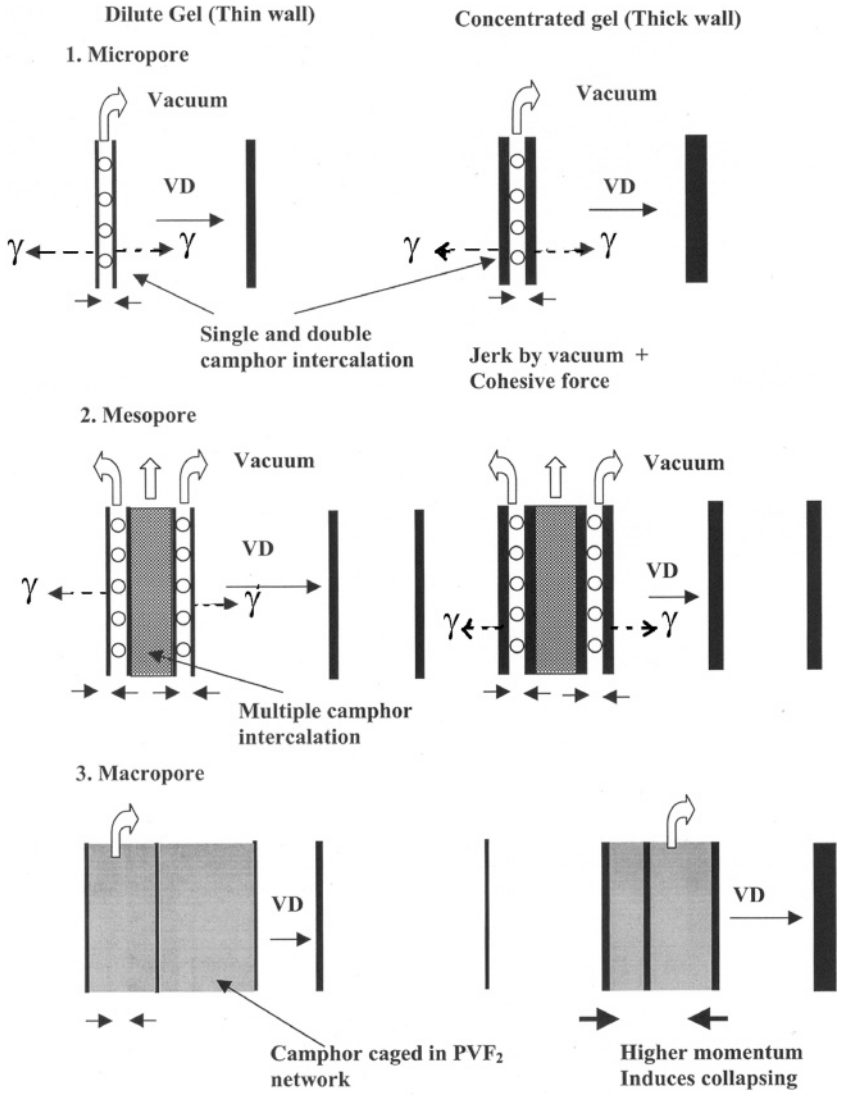

Figure 15. A schematic model for collapsing of pores during vacuum drying of PVF_2−camphor gel. γ denotes surface tensional force in micro- and mesopores, and this effect is not prominent in maropores because of small surface area (see text).

of VD samples are somewhat higher than those of CD samples for both 10% and 40% PVF_2 samples, indicating in the VD samples the pore walls are somewhat thicker than that of CD samples. The thicker pore walls in the VD samples may be produced due to collapsing of pores on vacuum drying.

Discussion

The effect of the drying method and concentration on the pore volume and surface area of the samples is summarized in Table 1. Both pore volume and surface area decrease (except for the surface area of VD sample) with increasing PVF_2 concentration in the gel. The anomaly of total surface area with concentration in VD samples might be due to the larger collapsing in P-10VD sample due to very dilute nature of the gel. The VD samples always exhibit decrease of surface area and pore volume than the corresponding CD samples, supporting significant collapsing in the VD samples.

To explain these results, we may use a schematic model presented in Figure 15. From the figure we have considered thin-walled and thick-walled pores; the latter is presented for the higher concentration of PVF_2 in the gel. The complexed solvent molecules (denoted by circles) are loosely bound by dipole−dipole interaction to the polymer chains. In vacuum the solvent molecules experience an upward pull, and consequently the thin PVF_2 layers experience a jerk. When all the solvent molecules are extracted, the jerk exerted by the applied vacuum (10^{-3} mmHg) attracts the semisolid polymer walls toward each other, and collapsing occurs due to combined forces of jerking and cohesive attraction of the polymer chains. When the distance between them is in the microporous region, the collapsing occurs completely as the cohesive force of attraction is operative in that range. The situation is applicable both for thin-walled and thick-walled pores.

As the distance between the semisolid polymer walls is increased, the mesoporous region (solvent is represented by a print pattern) is produced. Such mesopores may remain associated with micropores, and on extraction of solvent molecules from both the pores the micropores are collapsed, producing wider mesopores. Also, some squeezing of the empty walls of mesopores may occur toward each other due to jerking in vacuum, and collapsing of pores may take place reducing the population of mesopores. All the above possibilities are found in the case of mesopores. It should be mentioned here that surface tensional force (γ) of polymer strands try to oppose the effect of jerk by applied vacuum. This is because due to large surface area of micro- and mesopores the surface energy ($W = \gamma A$) is really large. But the jerking effect is strong enough to imbalance the surface tensional force in pore walls.

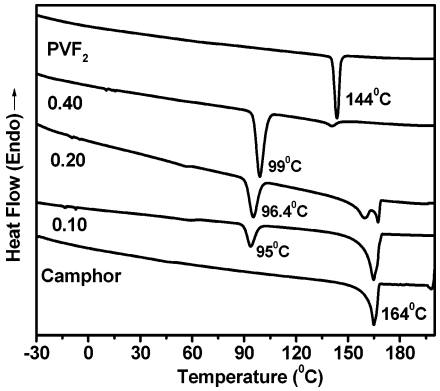

Figure 16. DSC cooling thermograms of CD and VD samples produced from the gels at indicated compositions along with that of pure PVF_2 and pure camphor at the cooling rate 5 °C/min.

The situation is really complicated in the case of macropores (solvent is presented as shaded area). Approximating the porosity of CD samples as the actual porosity present in the sample, it is inferred that in dilute gel the diameter of the macropores in VD samples has increased. This may be explained from the collapsing of micropores and some mesopores, which are lying on the walls of the macropores. The thin walls approach each other, forming a thicker wall of macropore and enlarge the diameter of original macropore. Some macropores may also collapse as evident from low-pressure distribution curve (Figure 3, inset). But the situation is quite different in the case of concentrated gel where a large number macropores are found to be collapsed. No definite explanation is known, and a possible explanation that may be appropriate is that the macropores are not very large in number in concentrated gel. As a result, the applied jerk by vacuum enables to induce much more momentum between the thicker macropore walls, making the pore walls to come closer to a distance where cohesive force of attraction is operative. So in the applied vacuum (10^{-3} mmHg) the higher PVF_2 concentration gel may show collapsing of macropores.

Now the question is why the CD samples have the possibility of retaining the porous structure in the gel. This is because cyclohexane has smaller size (5 Å) than the distance between the PVF_2 strands[13] (Scheme 1), and also it is not a good solvent or nonsolvent of PVF_2 as the gel does not swell or form precipitate in it. It behaves like a θ (theta) solvent of PVF_2. Further camphor is soluble in cyclohexane and gradually replaces the host camphor molecules. The process takes about 8−9 days time to replace camphor completely, indicating the process is almost thermodynamically reversible. Thus, there is no chance of any conformational change of PVF_2. The surface tensional effect of the polymer strands on the pore walls also assist here to retain the pore. During such solvent replacement the pore walls gradually transform into rigid solid state from the semisolid gel state. Such rigid system are then air-dried and finally dried in vacuum when no collapsing occurs due to gaining of rigidity. As a result, the porosity obtained from cyclohexane leached samples may be approximately considered as true porous structure present in PVF_2 camphor gel.

Now we would like to discuss about the cause of honeycomb-type pores in the P-40CD samples. Here, both the components are crystalline, and during the gel formation the systems are cooled from the melt when competitive crystallization occurs. It is evident from the Figure 16 that camphor crystallizes first, and a strong retardation of PVF_2 crystallization is observed. The crystallization of PVF_2 starts on the surface of a camphor crystal at center, and it grows at different directions (Figure 17). At the obstacle point imparted by camphor crystal, the PVF_2 lamella bends around its surface, making the knitting complete. After extracting the camphor this knitting pattern is obtained. Camphor may have a tendency of spherical crystal (spherulite) formation; as a result, honeycomb-type pores are produced. The sheetlike morphology appears in 10% gel because the camphor crystal size is very large and its concentration is also high. Consequently, PVF_2 grows through the niches of camphor crystals and fills the space. On extraction of camphor, sheet-type morphology of PVF_2 comes out.

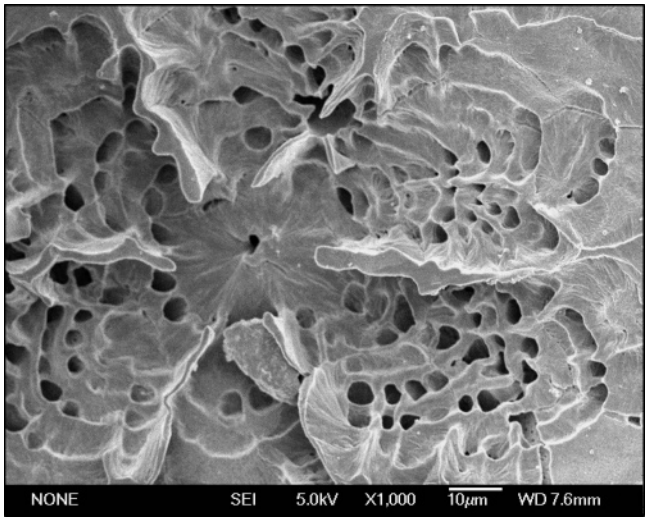

Figure 17. FESEM micrograph of P-40CD sample.

Conclusions

It may be concluded from this study that multiporous PVF_2 is prepared from its thermoreversible gels in camphor. Micropores are originated from the polymer−solvent complexation, and they have been attributed for single- and double-layer camphor complexation. The macropores are produced from the extraction of caged camphor molecules in the gel. Honeycomb types of pores are present in the dried PVF_2 camphor gel of higher PVF_2 concentration and faster crystallization of camphor than PVF_2 has been attributed for the honeycomb formation. There are interconnectivity between the pores of dried PVF_2 camphor system as evident from the hysteresis loop.

The drying method has a strong influence on the porosity, and on the interconnectivity of the pores. Vacuum drying decreases the porosity of the samples compared to that of cyclohexane replacement method of drying. Micropores are not at all observed in VD samples, but CD samples exhibit the presence of large amount of micropores. Mesopores are observed in both the CD and VD samples. For the samples with lower polymer concentration macropores are larger in size in VD sample than that in CD samples, but at higher concentration both the macropore size and population are reduced in the VD samples. The interconnectivity between the pores are also reduced in the VD sample than that of CD sample. The crystal structure is unaffected by the drying process, but the melting point of the crystals at the surface of pore wall are higher in VD than that in CD samples, suggesting the collapsing of pore wall on vacuum drying. The decrease of pore volume and surface area in vacuum drying process is due to collapsing of pores for mechanical jerking in the vacuum drying process.

Acknowledgment. We gratefully acknowledge IFCPAR Grant No. 2808-2 for financial support of the work. We also

gratefully acknowledge the help of Prof. B. Adhikari of IIT, Kharagpur, for helping in mercury intrusion porosometry experiment.

Supporting Information Available: Approximate models of single and double camphor molecule intercalation between two PVF_2 strands in PVF_2−camphor complex (Scheme 1); FT-IR spectra of P-40CD, P-40VD, PVF_2, and camphor (Figure 1); MIP hysteresis curves of P-10CD and P-10VD (Figure 2); BET adsorption isotherms of P-40CD and P-40VD (Figure 3); WAXS of CD and VD samples of PVF_2−camphor gels (Figure 4); DSC heating thermograms of P-10CD and P-40CD (Figure 5). This material is available free of charge via the Internet at http://pubs.acs.org.

References and Notes

(1) Rzayev, J.; Hillmyer, M. A. *Macromolecules* **2005**, *38*, 3.
(2) Soler-Illia, G. J de A. A.; Sanchez, C.; Lebeau, B.; Patarin, J. *Chem. Rev.* **2002**, *102*, 4093.
(3) Zhai, G.; Kang, E. T.; Neoh, K. G. *Macromolecules* **2004**, *37*, 7240.
(4) Hester, J. F.; Banerjee, P.; Won, Y. Y.; Akthakul, A.; Acar, M. H.; Mayes, A. M. *Macromolecules* **2002**, *35*, 7652.
(5) (a) Akthakul, A.; Salinaro, R. F.; Mayes, A. M. *Macromolecules* **2004**, *37*, 7663. (b) Ying, L.; Wang, P.; Kang, E. T.; Neoh, K. G. *Macromolecules* **2002**, *35*, 673.
(6) Guerra, G.; Manfredi, C.; Musto, P.; Tavone, S. *Macromolecules* **1998**, *31*, 1329.
(7) Xu, Y.; Zheng, D. W.; Tsai, Y.; Tu, K. N.; Zhao, B.; Liu, Q. Z.; Brongo, M.; Ong, C. W.; Choy, C. L.; Sheng, G. T. T.; Tung, C. H. *J. Electron. Mater.* **2001**, *30*, 309.
(8) Melosh, N. A.; Davidson, P.; Chemlka, B. F. *J. Am. Chem. Soc.* **2002**, *122*, 823.
(9) Goltner, C. G.; Henke, S.; Weissenbuger, M. C.; Antoniette, M. *Angew. Chem., Int. Ed.* **1998**, *37*, 613.
(10) Yang, H.; Coomls, N.; Ozin, G. A. *Nature (London)* **1997**, *386*, 692.
(11) Sing, K. S. W.; Everett, D. H.; Haul, R. A. W.; Moscou, L.; Pierotti, J.; Rouquerol, J.; Siemieniewska, T. *Pure Appl. Chem.* **1985**, *57*, 603.
(12) Dasgupta, D.; Nandi, A. K. *Macromol. Symp.* **2005**, *222*, 81.
(13) Dasgupta, D.; Nandi, A. K. *Macromolecules* **2005**, *38*, 6504.
(14) Malik, S.; Roizard, D.; Guenet, J. M. *Macromolecules* **2006**, *39*, 5957.
(15) Ding, Y.; Erlebacher, J. *J. Am. Chem. Soc.* **2003**, *125*, 7772.
(16) Smått, J. H.; Schunk, S.; Lindén, M. *Chem. Mater.* **2003**, *15*, 2354.
(17) Huang, L.; Wang, Z.; Sun, J.; Miao, L.; li, Q.; Yan, Y.; Zhao, D. *J. Am. Chem. Soc.* **2000**, *122*, 3530.
(18) Rhodes, K. H.; Davis, S. A.; Caruso, F.; Zhang, B.; Mann, S. *Chem. Mater.* **2000**, *12*, 2832.
(19) Yin, J. S.; Wang, J. L. *Appl. Phys. Lett.* **1999**, *74*, 2629.
(20) Lebeau, B.; Fowler, C. E.; Mann, S.; Foucer, C.; Charleux, B.; Sanchez, C. *J. Mater. Chem.* **2000**, *10*, 2105.
(21) Guenet, J. M.; Ray, B.; Elhasri, S.; Marie, P.; Thierry, A. *NATO Sci. Ser. IV*: *Earth Environ. Sci.* ***2003***, *24*, *191*.
(22) Dasgupta, D.; Manna, S.; Malik, S.; Rochas, C.; Guenet, J. M.; Nandi, A. K. *Macromolecules* **2005**, *38*, 5602.
(23) Roerdink, E.; Challa, G. *Polymer* **1980**, *21*, 509.
(24) Belke, R. E.; Cabasso, I. *Polymer* **1988**, *29*, 1831.
(25) Guenet, J. M.; McKenna, G. B.; *Macromolecules* **1988**, *21*, 1752.
(26) Lovinger, A. J. In *Developments in Crystalline Polymers, 1*; Basset, D. C., Ed.; Elsevier Applied Science: London, 1981; p 195.
(27) Li, K. *Chem. Eng. Technol.* **2002**, *25*, 2.
(28) (a) Chen, Y.; Ying, l.; Yu, W.; Kang, E. T.; Neoh, K. G. *Macromolecules* **2003**, *36*, 9451. (b) Wang, P.; Tan, K. L.; Kang, E. T.; Neoh, K. G. *J. Mater. Chem.* **2001**, *11*, 783.
(29) Prest, Jr., W. M.; Luca, D. J. *Bull. Am. Phys. Soc.* **1974**, *19*, 217.
(30) Nandi, A. K.; Mandelkern, L. *J. Polym. Sci., Polym. Phys.* **1991**, *B29*, 1287.
(31) Washburn, E. W. *Phys. Rev.* **1921**, *17*, 273.
(32) Moro, F.; Böhni, H. *J. Colloid Interface Sci.* **2002**, *246*, 135.
(33) Barrett, E. P.; Joyner, L. G.; Halenda, P. P. *J. Am. Chem. Soc.* **1951**, *73*, 373.
(34) Horvath, G.; Kawazoe, K. J. *J. Chem. Eng. Jpn.* **1983**, *16*, 470.
(35) León, C. A.; León, Y. *Adv. Colloid Interface Sci.* **1998**, *76*−*77*, 341.
(36) Kuang, D.; Brezesinski, T.; Smarsly, B. *J. Am. Chem. Soc.* **2004**, *126*, 10534.
(37) Zhang, H.; Sun, J.; Ma, D.; Bao, X.; Klein-Hoffmann, A.; Weinberg, G.; Su, D.; Schlogl, R. *J. Am. Chem. Soc.* **2004**, *126*, 7440.
(38) Dikshit, A. K.; Nandi, A. K. *Macromolecules* **1998**, *31*, 8886.
(39) Mal, S.; Nandi, A. K. *Polymer* **1998**, *39*, 6301.
(40) Chou, C.-M.; Hong, P.-D. *Macromolecules* **2003**, *36*, 7331.
(41) Lando, J. B.; Doll, W. W. *J. Macromol. Sci., Phys.* **1968**, *2*, 205.
(42) Hasegawa, R.; Takahashi, Y.; Chatani, Y. *Polym. J.* **1972**, *3*, 600.
(43) Guerra, G.; Karasz, F. E.; MacKnight, W. J. *Macromolecules* **1986**, *19*, 1935.
(44) Mandelkern, L. In *Comprehensive Polymer Science*; Allen, G., Ed.; Pergamon Press: Oxford, 1989; Vol. 2, p 363.

MA062709H